Journal of Advanced Ceramics
2012, 1(4): 274-282
DOI: 10.1007/s40145-012-0026-9 ISSN 2226-4108

Research Article

Modeling the crystallographic structure of $Ho(Ni,Co,Mn)O_{3\pm\delta}$ perovskite-type manganite

C. Morilla-Santos[a], F. F. Ferreira[b], W. H. Schreiner[c], O. Peña[d], P. N. Lisboa-Filho[e,*]

[a]*UNESP - Univ Estadual Paulista, POSMAT - Programa de Pós-Graduação em Ciência e Tecnologia de Materiais, Bauru, Brazil*
[b]*UFABC - Universidade Federal do ABC - Centro de Ciências Naturais e Humanas, Santo André, Brazil*
[c]*UFPR - Universidade Federal do Paraná, Departamento de Física, Curitiba, Brazil*
[d]*Sciences Chimies de Rennes UMR 6226, Université de Rennes 1, Rennes, France*
[e]*UNESP - Univ Estadual Paulista, Faculdade de Ciências, Departamento de Física, Bauru, Brazil*

Received: September 1, 2012; Accepted: November 3, 2012

Abstract: Crystallographic and microstructural properties of $Ho(Ni,Co,Mn)O_{3\pm\delta}$ perovskite-type multiferroic material are reported. Samples were synthesized with a modified polymeric precursor method. The synchrotron X-ray powder diffraction (SXRPD) technique associated to Rietveld refinement method was used to perform structural characterization. The crystallographic structures, as well as microstructural properties, were studied to determine unit cell parameters and volume, angles and atomic positions, crystallite size and strain. X-ray energies below the absorption edges of the transition metals helped to determine the mean preferred atomic occupancy for the substituent atoms. Furthermore, analyzing the degree of distortion of the polyhedra centered at the transitions metal atoms led to understanding the structural model of the synthesized phase. X-ray photoelectron spectroscopy (XPS) was performed to evaluate the valence states of the elements, and the tolerance factor and oxygen content. The obtained results indicated a small decrease distortion in structure, close to the $HoMnO_3$ basis compound. In addition, the substituent atoms showed the same distribution and, on average, preferentially occupied the center of the unit cell.

Key words: crystallographic structure; X-ray powder diffraction; Rietveld refinement; manganites

1 Introduction

Multiferroic manganites are a unique class of strongly correlated materials having very rich magnetic phase diagrams, including competitive and cooperative phenomena. In the absence of an applied magnetic field, manganites are insulators; however, small magnetic fields induce metal insulator transitions [1].

Although the crystal structure and basic physical phenomena of such compounds have been known since the 1950s, several questions remain. Some are related to site occupancy and the effects on the magnetic response of these manganites.

* Corresponding author.
E-mail: plisboa@fc.unesp.br

Substitutions of divalent and trivalent transition metals at the manganese site have been performed on $REMnO_3$ (RE, rare-earth) perovskite-type compounds. The literature reports studies in which substitutions are made with cobalt or nickel atoms in systems such as $RE(Mn,TM)O_3$ (TM, transition metal) [2,3]. These studies, concerning synthesis and structural and magnetic characterization, have been predominantly obtained using solid state techniques. This highlights the role of chemical elements in the structure's formation. The use of different RE and TM allows structures with different symmetries and with several degrees of distortion to be obtained, which in turn dictate the magnetic properties of the compounds [2-5]. The properties of polycrystalline samples as well as single crystals were studied [6].

Manganite oxides have the chemical formula ABO_3, in which trivalent atoms occupy the A site and manganse atoms occupy the B site. The structural model of an ideal cubic perovskite corresponds to the metals atoms occupying the center and the vertices, and oxygen atoms occupying the faces of the cube as shown in Fig. 1(a). The cohesion of the structure is due to chemical bonds between manganese and oxygen. Each manganese atom is surrounded by oxygen atoms sitting at the vertices of octahedrons that reflect the degree of structural distortion. For an ideal cubic perovskite structure, the polyhedra centered on the B site are not distorted, as shown in Fig. 1(b). In terms of structural optimization, the degree of distortion observed by the octahedral BO_6 can be described in terms of the ionic radii of the elements and by Jahn-Teller effect. Since *Ra* is the ionic radius of the element in site A, *Rb* is the ionic radius of element in site B, and *Ro* is the ionic radius of oxygen, a tolerance factor can be defined as [7]:

$$f = \frac{Ra + Ro}{Rb + Ro} \cdot \frac{1}{\sqrt{2}}$$

This factor qualitatively describes the degree of distortion of the experimental structure compared to the ideal cubic perovskite structure. For the ideal case, we have $f = 1$, and O-B-O angles equal to 180°. Structural changes lead to a shift in the tolerance factor: for rhombohedral symmetry, we have $0.96 < f < 1$, and for orthorhombic symmetry, we have $f < 0.96$ [8]. There are also reports that the perovskite structure is guaranteed stable with $0.89 < f < 1.2$ [9].

In the families of compounds where transition metals replace manganese atoms, an important experimental factor must be considered. When the chemical elements are situated near each other in the periodic table, more than one wavelength may be necessary to analyze the X-ray diffraction data, because chemical elements may have similar atomic scattering factor values when using a conventional radiation source. Thus, differentiating the sites occupied by substituent atoms preferentially becomes difficult [10,11]. For these cases, the use of synchrotron light is a key point for crystallographic characterization of the compound. In this sense, the use of X-ray energies below the absorption edge of transition metals gives a contrast in the atomic scattering factors, and shows the preferred occupation of the transition metals in the structure [10-13].

Most of the studies on substitutional effects in manganites have been focused on substituting the trivalent A-site ion by a divalent ion to induce ferromagnetism and conductivity through Mn3p and Mn4p double exchange interactions. Otherwise, on yttrium-based manganites, some effects of B-site substitution, replacing some Mn ions by 3d-magnetic ions, such as Co, Ni or Cu were investigated [14]. It was shown that an almost perfect atomic order of Mn4p and Ni2p can be detected in the half-substituted compound $YMn_{0.5}Ni_{0.5}O_3$. Also, the authors claimed that those ions were randomly distributed in another composition of the $Y(Mn, Ni)O_3$ system.

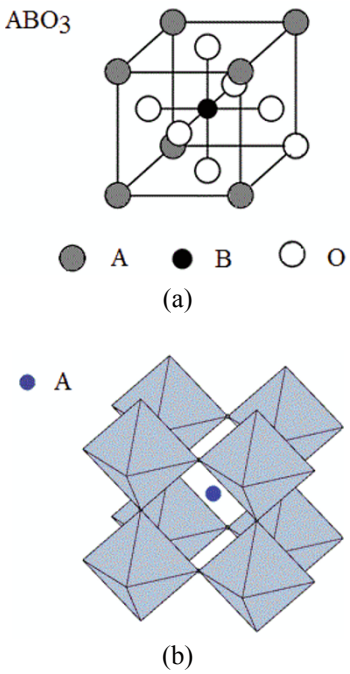

Fig. 1 (a) Ideal cubic perovskite; (b) Octahedral sites (BO_6).

A special case of manganite compounds is $HoMnO_3$ [15,16] which presents a rich magnetic diagram that includes below the paramagnetic state, at $T_N = 41$ K an incommensurate AFM ordering that consists of a sinusoidal modulated magnetic structure concerning only to the Mn^{3+} magnetic moments. Also, below $T = 22$ K, Ho^{3+} magnetic moments also become ordered superimposed onto the ordered Mn sublattice and it is known that the magnetic ordering in Ho^{3+} ions is associated with Ho-O-Ho superexchange interactions. Finally, a commensurate magnetic structure is stable down to 1.5 K.

Other two interesting cases are $HoCoO_3$ which crystallizes in the orthorhombic Pnma space group and Ho^{3+} ions turn out to be antiferromagnetically ordered below $T_N = 1.8$ K [17], and $HoNiO_3$ in that rare-earth sublattice orders with a different propagation vector from the Ni one, indicating that in this compound the rare-earth and the transition-metal sublattices are magnetically decoupled at least below 3 K and the Ho-Ho interactions are stronger than the possible Ni-Ho interactions [18].

Considering the complexity of substitutional effects in this perovskite and its effects on magnetic correlations, the aim of this study was to determine the crystal structure of $HoNi_{0.25}Co_{0.25}Mn_{0.50}O_{3\pm\delta}$ perovskite-type, synthesized with Pechini method. X-ray photoelectron spectroscopy (XPS) allowed us to estimate the oxidation state that the elements presented, and therefore to estimate the oxygen stoichiometry with charge balance considerations. The use of X-ray powder diffraction associated with Rietveld refinement method allowed the unit cell parameters, volume, atomic positions, degree of distortion of the structure, and a schematic view for the unit cell to be determined. Moreover, microstructural characteristics dependent on the synthesis process were also determined.

2 Experimental details

The modified polymeric precursor method has been widely used in synthesizing oxide compounds. Purity, homogeneity, low level of agglomeration, and small particle size distribution are some of the advantages of this method compared to solid state reaction. Moreover, the possibility of variations in sol-gel methodology, and the use of relatively lower temperatures for heat treatment are factors to be considered [19-21].

To synthesize the $HoNi_{0.25}Co_{0.25}Mn_{0.50}O_{3\pm\delta}$ phase, Ho_2O_3, $MnCO_3$ and $Co(NO_3)_2{\cdot}6H_2O$ in stoichiometric amounts were dissolved in deionized water at 60 ℃, followed by a metal/carboxylic acid solution of molar ratio of 1 : 3. For dissolution of oxide and carbonate, nitric acid was added to solutions. Subsequently, the obtained solution was further diluted in another solution containing citric acid dissolved in deionized water for chelation of metals. After two hours in constant agitation at 70 ℃, the solution was polymerized by adding ethylene glycol at a carboxylic acid/polyalcohol mass ratio of 60 : 40. The pH of solution was then adjusted to a value of 3, with the addition of ethylenediamine, and after 24 h in constant agitation at temperatures around 80 ℃ to remove the solvent, a polymeric resin was formed. To remove the organic portion, the gel was heated at 350 ℃/4 h [20], and subsequently at 500 ℃/4 h and 900 ℃/20 h in order to obtain a crystalline phase.

To quantify the oxidation states of the transition metals, XPS analysis was performed. The spectra were obtained by using a VG ESCA 3000 system, collected with MgKα radiation and resolution of 0.8 eV. The correction in spectra was performed through C1s peak with binding energy of 284.5 eV, and the concentration of valence state was determined with the deconvolution process using XI_SDP 3.0 software. After the valence states were determined, the tolerance factor was calculated based on the effective ionic radii of the rare-earth metals, the transition metals, and the oxygen atoms. Finally, it was possible to estimate the stoichiometry of oxygen, with charge balance considerations.

To determine whether secondary phases were present, as well as to generate the crystallographic information file (CIF), XRD analyses were performed in the conventional diffractometer Rigaku D/MAX 2100PC. In this analysis, radiation CuKα, 40 kV, 20 mA, a divergence slit of 1°, a receiving slit of 0.3 mm, a nickel filter, a step of 0.02°, a scan angle range of 10° to 100°, and a fixed time of 1 s/step were used. Unit cell parameters and volume were determined with the indexing process, achieved through the software Crysfire suite [22] and the analytical process of indexing [23].

The International Tables for Crystallography [24] were consulted to confirm the space group and systematic absences. Atomic positions were obtained from the crystallographic information file 157395-ICSD ($HoMnO_3$ basis compound). Combining XRD and XPS data, Rietveld refinement was performed

using the GSAS software program [25] and the interface of EXPGUI [26].

After a CIF file of the synthesized phase was generated, the sample was analyzed at the X-ray powder diffraction beamline of the Brazilian Synchrotron Light Laboratory (D10B-XPD-LNLS, Campinas, SP, Brazil). To estimate the substituent atoms occupancy, the analysis was performed with X-ray energies below the nickel (1.4876 Å), cobalt (1.6130 Å), and manganese (1.8967 Å) absorption edges. A Si(111) crystal monochromator and Ge(111) crystal analyzer were used with synchrotron radiation, and a polycrystalline standard Si(111) sample was used for wavelength refinements.

3 Results and discussion

Table 1 presents information about the process of indexing carried out by using the Crysfire software and analytical methods, as well as calculated unit cell parameters, atomic positions and the space group taken from the crystallographic information file ICSD-157395 ($HoMnO_3$ basis compound). After manganese was substituted with nickel and cobalt atoms, information about the position and occupation of the substituent atoms was also included in Table 1. The indexing procedure was particularly useful, since the literature reported the existence of a strong competition between the hexagonal ($P6_3cm$) and orthorhombic (Pbnm) symmetries for $HoMnO_3$ [27]. In our case, the synthesized phase present has an orthorhombic structure.

The survey spectrum from 0 to 1100 eV range showed the displacement of 11.7 eV, in relation to the C1s peak. After correction, the deconvolution process allowed us to estimate the oxidation states of transition metals and their concentrations, which were obtained from the binding energy values described in the Handbook of X-ray Photoelectron Spectroscopy [28]. In Fig. 2, Fig. 3 and Fig. 4 XPS analysis are presented, performed in the binding energy region of Ni2p, Co2p and Mn2p spectra. Besides, the results of decovolutions are presented in Table 2. Considering the concentration of valence state ions, it was determined that the synthesized phase has a charge balanced formula $Ho^{3+}Ni^{2+}_{(0.25)}Co^{2+}_{(0.13)}Co^{3+}_{(0.12)}Mn^{3+}_{(0.30)}Mn^{4+}_{(0.20)}O^{2-}_{3\pm\delta}$. Based on the balance of charge, it was estimated that $3\pm\delta$ has the value around 2.91, and the occupancy for oxygen atom labeled as O_2 is approximately 0.955, the value presented in Table 1. Furthermore, from the effective ionic radii of ions, the calculated tolerance factor was 0.796. This result reinforced the possibility of the formation of a phase with orthorhombic symmetry [8]. What's more, although the value was outside the range ensuring the stability of the perovskite structure [9], the refinement showed that the synthesized phase has the mentioned structure.

Using the values in Table 1, conventional radiation data was refined, and a CIF file was generated for the crystallographic phase $HoNi_{0.25}Co_{0.25}Mn_{0.50}O_{2.91}$, to be used in further refinements with the data obtained from the use of synchrotron radiation. The refinement is illustrated in Fig. 5, where it is possible to observe the

Table 1 Initial crystallographic information used to perform Rietveld refinements using a conventional data

a (Å)	*b* (Å)	*c* (Å)	*α* (º)	*β* (º)	*γ* (º)
5.2066	5.5515	7.4617	90	90	90*
5.2201	5.5205	7.4387**			
Symmetry	Orthorhombic		Space group	Pbnm	
Atom	*x*	*y*	*z*	Occupancy	Multiplicity
Ho	0.9828	0.0836	0.2500	1.000	4
Ni	0.5000	0	0	0.250	4
Co	0.5000	0	0	0.250	4
Mn	0.5000	0	0	0.500	4
O1	0.0936	0.4372	0.2500	1.000	4
O2	0.6965	0.3363	0.0440	0.955	8

*: Crysfire: TP TAUP. TREOR90/log. Considered to generate the crystallographic file for the initial refinement.

**: Analytical indexing considering orthorhombic symmetry.

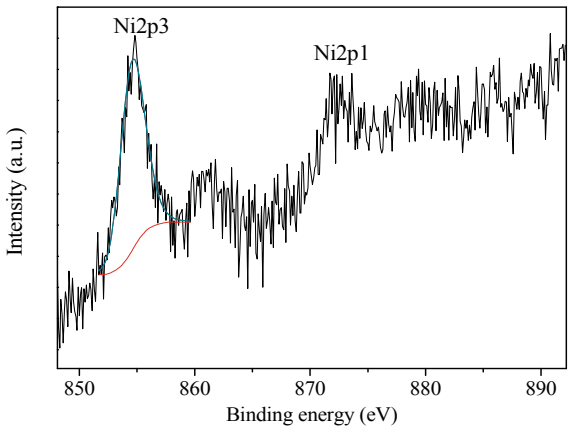

Fig. 2 XPS analyses for $HoNi_{0.25}Co_{0.25}Mn_{0.50}O_{3\pm\delta}$ sample, Ni2p spectrum.

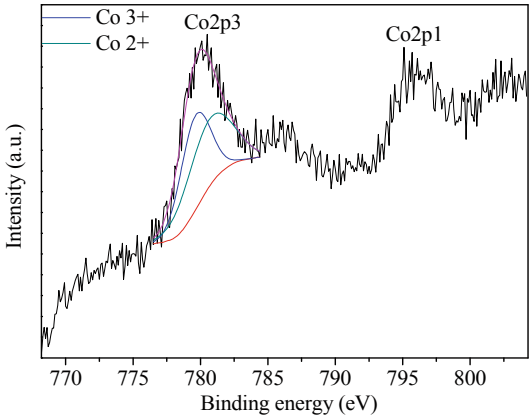

Fig. 3 XPS analyses for $HoNi_{0.25}Co_{0.25}Mn_{0.50}O_{3\pm\delta}$ sample, Co2p spectrum.

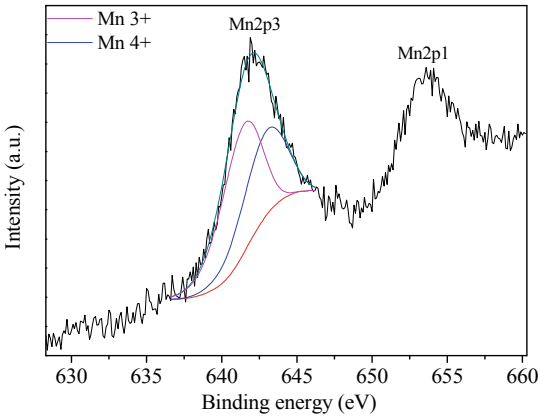

Fig. 4 XPS analyses for $HoNi_{0.25}Co_{0.25}Mn_{0.50}O_{3\pm\delta}$ sample, Mn2p spectrum.

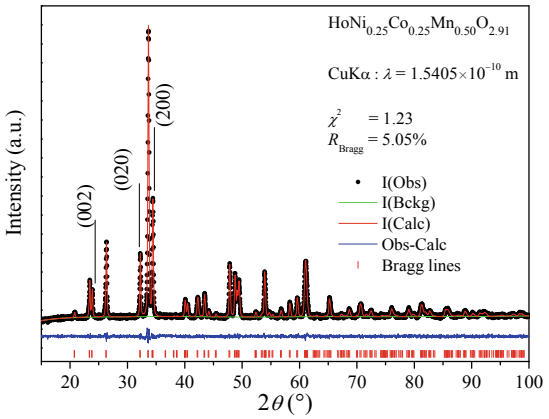

Fig. 5 Rietveld refinement of analysis collected using a conventional radiation.

Table 2 Information about valence state of transitions metals

	Valence state	Binding energy (eV)	Concentration (%)
Ni2p3/2	2+	854.8	100.0
Co2p3/2	2+	781.2	55.1
	3+	779.9	44.9
Mn2p3/2	3+	641.7	59.6
	4+	643.2	40.4

XPS statistical parameter (χ^2): Ni2p3/2 (5.82), Co2p3/2 (6.05), Mn2p3/2 (5.20).

experimental data (black), the calculated data (red), the background line (green), and the residue (blue). The vertical red line represents Bragg lines, and the χ^2 and R_{Bragg} parameters represent the statistical indicators of refinement. There are no evident signs of secondary phases, or remnants of the starting reagents. This result is also evidenced by the absence of the main peak of holmium oxide, around 29.14°. For this refinement, the instrumental broadening values were analyzed through Rietveld refinement of an Y_2O_3 standard sample, treated at 1200 ℃/72 h.

Figures 6-8 show Rietveld refinements, collected using synchrotron radiation with energies below the absorption edges of nickel, cobalt and manganese respectively. For these analyses, the refinement for each wavelength was evaluated through Rietveld refinement of a polycrystalline standard Si(111) sample, acquired from the National Institute of Standards and Technology (NIST), USA, SRM 640c. In addition, anomalous scattering factors (f' and f'') provided by FPrime for Windows V1 software [29] were used, depending on the wavelength considered.

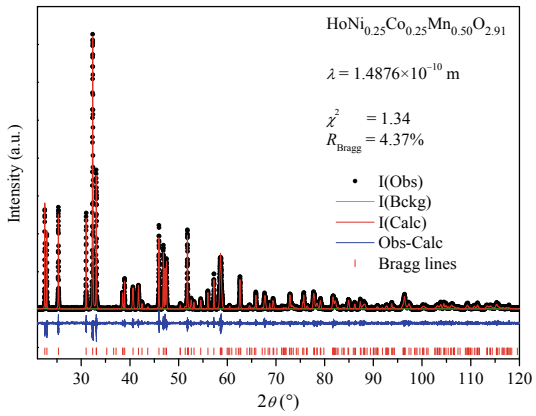

Fig. 6 Rietveld refinement of the $HoNi_{0.25}Co_{0.25}Mn_{0.50}O_{2.91}$ sample using synchrotron data measured with an X-ray of $\lambda = 1.4876$ Å.

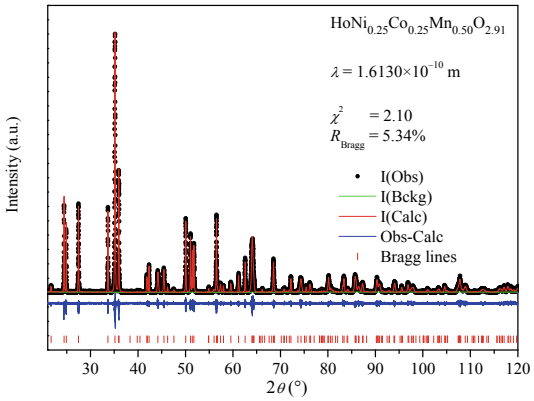

Fig. 7 Rietveld refinement of the $HoNi_{0.25}Co_{0.25}Mn_{0.50}O_{2.91}$ sample using synchrotron data measured with an X-ray of $\lambda = 1.6130$ Å.

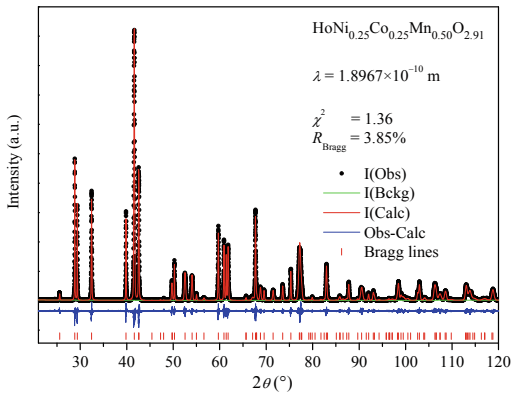

Fig. 8 Rietveld refinement of the $HoNi_{0.25}Co_{0.25}Mn_{0.50}O_{2.91}$ sample using synchrotron data measured with an X-ray of $\lambda = 1.8967$ Å.

Similarly to what was done for the refinement of Fig. 5, a polynomial shifted Chebyschev background function with 6 terms was used for synchrotron data. The profile of the diffraction peaks was modeled with a pseudo-Voigt function parameterized by Thompson [30], and the asymmetry correction was done using the model proposed by Finger [31]. Constraints were used for the transition metals, one for the atomic displacement parameter, and another concerning the replacement of manganese with nickel and cobalt atoms. In each analysis, we refined the background, scale, unit cell parameters, atoms positions, atomic displacements, surface roughness, and parameters related to microstructure. Table 3 summarizes the main features of the unit cell of phase $HoNi_{0.25}Co_{0.25}Mn_{0.50}O_{2.91}$ refined with data from synchrotron radiation. There was not observed preferred orientation.

Table 3 Results of Rietveld refinement using synchrotron radiation data

Structure information			
Molecular formula	$HoNi_{0.25}Co_{0.25}Mn_{0.50}O_{2.91}$		
Chemical synthesis	Pechini method		
Crystal information			
Symmetry	Orthorhombic		
Space group	Pbnm(62)		
Unit-cell parameters	a = 5.22(89) Å, b = 5.56(79) Å, c = 7.48(48) Å		
Unit-cell volume	V= 217.921 (1)Å^3		
Atomic coordinates			
Atom	x	y	z
Ho	0.98(11)	0.071(47)	0.25
Ni	0.50	0	0
Co	0.50	0	0
Mn	0.50	0	0
O1	0.10(14)	0.46(18)	0.25
O2	0.68(74)	0.30(11)	0.055(48)
Atomic angles			
TM-O1-TM	145.67º		
TM-O2-TM	144.38º		
Statistical information			
λ(Å)	χ^2	R_{Bragg} (%)	
1.4876 ± 0.000029	1.34	4.37	Fig. 6
1.6130 ± 0.000020	2.10	5.34	Fig. 7
1.8967 ± 0.000023	1.36	3.85	Fig. 8

Figure 9 illustrates two perspective views of $HoNi_{0.25}Co_{0.25}Mn_{0.50}O_{2.91}$ unit cell, generated using the DrawXTL 5.5 software from synchrotron refined data. In Fig. 9(a), holmium atoms (blue spheres), oxygen atoms (red spheres), and polyhedra centered on transition metal atoms are observed. The TM-O1-TM (TM = Ni, Co or Mn) angle is about 145.67°, and TM-O2-TM angle is about 144.38°. These values are close to the value of 144.1° reported for the $HoMnO_3$ phase [15]. These values for interatomic angles are presented in Table 3, and demonstrate the degree of distortion with respect to the ideal cubic perovskite, where the angles are equal to 180°. Furthermore, the angles θ_1 and θ_2 presented in Fig. 9(b) have values around 64.61° and 115.39° respectively, in contrast with the 90° of an ideal cubic perovskite. A comparison with $HoMnO_3$ whose tolerance factor is around 0.796, shows that this synthesized phase has a slightly higher distortion. Although the difference is relatively small, a comparison of the unit cell parameters showed that the volume of the synthesized phase is 3.61% lower than $HoMnO_3$. This difference can be attributed to the presence of transition metals with different valence states, and to incomplete oxygen stoichiometry.

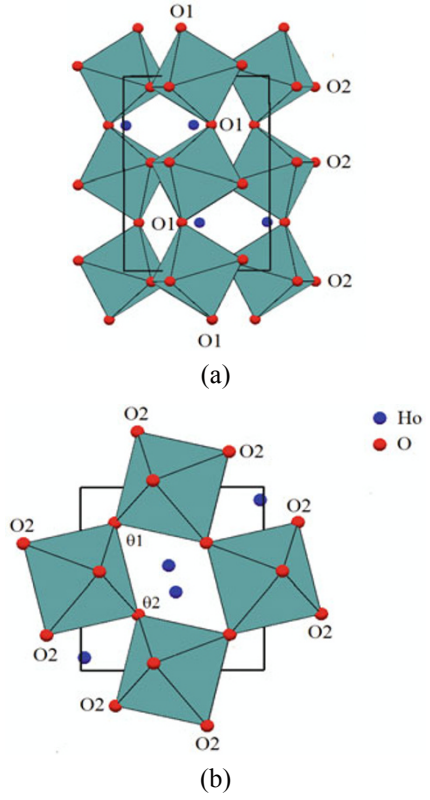

Fig. 9 Refined unit cell of the phase $HoNi_{0.25}Co_{0.25}Mn_{0.50}O_{2.91}$.

To determine the preferred occupation of the substituent atoms, integrated intensities were analyzed in the planes (200), (020) and (002) at the three wavelengths used. This situation reflected the differences in integrated intensities, and therefore the determination of the preferred transition metal occupation site. A comparison of these values showed that on the average the occupation of manganese atoms in the plane that crosses the *z*-axis in the middle is about 40%. In this plane, the concentration of substituent atoms is equivalent. Moreover, an average of 46.6% of the substituent atoms presented in the unit cell occupy the top and bottom of the unit cell.

Table 4 presents the anisotropic microstructure analysis performed using synchrotron data. The mean crystallite size, 441 nm×201 nm, was determined based on equations for the bimodal crystallite size [25]. Also in Table 4, the microstrain values to the (111), (200), (020) and (002) planes, calculated considering Laue symmetry and Stephens formulation [32], show an anisotropic microstrain.

4 Conclusions

In this work, we determined the crystallographic and physical properties of the $HoNi_{0.25}Co_{0.25}Mn_{0.50}O_{2.91}$ sample, synthesized with Pechini method. The proposed model for Rietveld refinement, with data obtained through diffraction and X-ray spectroscopy techniques, showed that the synthesized phase has the perovskite structure. In the process of atomic substitution, a reduction in the unit cell volume, and small changes in the atomic positions and angles were observed. Compared with the $HoMnO_3$ base compound, the synthesized phase showed a small increase in the structural distortion. These structural changes are assigned to the presence of several ions of different ionic radii and the oxygen content. Synchrotron radiation displayed that the substituent atoms showed the same distribution, and on average, preferentially

Table 4 Mean crystallite size and microstrain of $HoNi_{0.25}Co_{0.25}Mn_{0.50}O_{2.91}$ sample

Wavelength	Crystallite size (Standard deviation $\pm10^{-8}$ nm)	Plane	Microstrain
1.613 01 Å	445 nm × 208 nm	(111)	3.393×10^{-3}
1.896 70 Å	436 nm × 185 nm	(200)	2.072×10^{-3}
1.487 63 Å	443 nm × 210 nm	(020)	1.802×10^{-3}
Mean crystallite size	441 nm × 201 nm	(002)	2.069×10^{-3}

occupied the center of the unit cell. The synthesis by the chemical method was successful; moreover, large crystallite size and small values for microstrain were observed.

Acknowledgement

The authors acknowledge the financial support of the Brazilian funding agencies CNPq and FAPESP, and thank for CAPES-COFECUB exchange program (706/2011).

References

[1] Dagotto E, Burgy J, Moreo A. Nanoscale phase separation in colossal magnetoresistance materials: Lessons for the cuprates. *Solid State Communications* 2003, **126**: 9-22.

[2] Antunes AB, Ceretti M, Paulus W, *et al*. Magnetic domains and anisotropy in single crystals of $Er(Co,Mn)O_3$. *J Magn Magn Mater* 2008, **320**: e69-e72.

[3] Barahona P, Peña O, Antunes AB, *et al*. Magnetic properties of Mn-substituted $GdCo_xMn_{1-x}O_3$ and $LaCo_xMn_{1-x}O_3$. *J Magn Magn Mater* 2008, **320**: e61-e64.

[4] Antunes AB, Gil V, Moure C, *et al*. Magnetic properties of $Er(Co,Mn)O_3$ perovskites. *J Eur Ceram Soc* 2007, **27**: 3927-3930.

[5] Moure C, Tartaj J, Moure A, *et al*. Crystalline structure of the manganites solid solution $RE(Me,Mn)O_3$, (RE=Gd, Er; Me=Ni, Co). *Bol Soc Esp Ceram* 2009, **48**: 199-204.

[6] Gatalskaya VI, Shiryaev SV, Barilo SN, *et al*. Low-temperature magnetic properties of $HoMn_{0.5}Co_{0.5}O_3$ single crystals. *Physics of the Solid State* 2005, **47**: 1265-1269.

[7] Goldschmidt VM. *Geochemische Verteilungsgesetze der Elemente*. Jacob Dybwad-Verlag Oslo, 1927-1928: vol Ⅶ-Ⅷ.

[8] Tokura Y, Tomioka Y. Colossal magnetoresistive manganites. *J Magn Magn Mater* 1999, **200**: 1-23.

[9] Coey JMD, Viret M, von Molnár S. Mixed-valence manganites. *Adv Phys* 1999, **48**: 167-293.

[10] Ferreira FF, Granado E, Carvalho Jr W, *et al*. X-ray powder diffraction beamline at D10B of LNLS: Application to the Ba_2FeReO_6 double perovskite. *J Synchrotron Rad* 2006, **13**: 46-53.

[11] Ferreira FF, Bueno PR, Setti GO, *et al*. Resonant X-ray diffraction as a tool to calculate mixed valence ratios: Application to Prussian blue materials. *Appl Phys Lett* 2008, **92**: 264103/1-264103/3.

[12] Rietveld HM. A profile refinement method for nuclear and magnetic structures. *J Appl Cryst* 1969, **2**: 65-71.

[13] Young RA. *The Rietveld Method*. Oxford: Oxford University Press, 1993.

[14] Mouallem-Bahout M, Roisnel T, Bourée F, *et al*. Neutron diffraction evidence for a cationic order in the $REMn_{0.5}Ni_{0.5}O_3$ (RE = La, Nd) and $YMn_{0.5}Co_{0.5}O_3$ perovskites. *Prog Solid State Chem* 2007, **35**: 257-264.

[15] Brinks HW, Rodriguez-Carvajal J, Fjellvag H, *et al*. Crystal and magnetic structure of orthorhombic $HoMnO_3$. *Phys Rev B* 2001, **63**: 094411/1-094411/12.

[16] Muñoz A, Casáis MT, Alonso JA, *et al*. Complex magnetism and magnetic structures of the metastable $HoMnO_3$ perovskite. *Inorg Chem* 2001, **40**: 1020-1028.

[17] Jadhao VG, Singru RM, Rama RG, *et al*. Effect of the rare earth ion on the spin state equilibria in perovskite rare earth metal cobaltates. Yttrium trioxocobaltate (Ⅲ) and erbium trioxocobaltate (Ⅲ). *J Chem Soc* 1975, **71**: 1885-1893.

[18] Fernández-Díaz MT, Alonso JA, Martınez-Lope MJ, *et al*. Magnetic structure of the $HoNiO_3$ perovskite. *Phys Rev B* 2001, **64**: 144417/1-144417/5.

[19] Pechini MP. Method of preparing lead and alkaline earth titanates and niobates and coating method using the same to form a capacitor. U. S. Patent, 3330697, July 1967.

[20] Kakihana M. Sol-gel preparation of high temperature superconducting oxides. *Journal of Sol-Gel Science and Technology* 1996, **6**: 7-55.

[21] Tai LW, Lessing PA. Modified resin-intermediate processing of perovskite powders: Part I. Optimization of polymeric precursors. *J Mater Res* 1992, **7**: 502-510.

[22] Shirley R. *The Crysfire System for Automatic Powder Indexing*: *Users Manual*. England: The Lattice Press, 2000.

[23] Cullity BD. *Elements of X-ray Diffraction*. New Jersey: Prentice Hall, 2001.

[24] *Internationl Tables for Crystallography*, *Volume A-Space Group Symmetry*. D. Reidel Publishing Company, 1983.

[25] Larson AC, von Dreele RB. *General Structure Analysis System* (*GSAS*). Los Alamos National Laboratory Report LAUR 86-748, 2004.

[26] Toby BH. EXPGUI, a graphical user interface for GSAS. *J Appl Cryst* 2001, **34**: 210-213.

[27] Brinks HW, Fjellvag H, Kjekshus A. Synthesis of metastable perovskite-type $YMnO_3$ and $HoMnO_3$. *J*

Solid State Chem 1997, **129**: 334-340.

[28] Moulder JF, Stickle WF, Sobol PE, *et al*. Handbook of X-ray Photoelectron Spectroscopy. Eden Prairie: Perkin-Elmer Corporation, 1995.

[29] von Dreele RB. Program FPrime for Windows 1.0 for calculating real and anomalous X-ray dispersion coefficients. 1994. http://www.ccp14.ac.uk/ccp/ccp14/ftp-mirror/gsas/public/gsas/windows/.

[30] Thompson P, Cox DE, Hastings JB. Rietveld refinement of Debye-Scherrer synchrotron X-ray data from $A1_20_3$. *J Appl Cryst* 1987, **20**: 79-83.

[31] Finger LW, Cox DE, Jephcoat AP. Acorrection for powder diffraction peak asymmetry due to axial divergence. *J Appl Cryst* 1994, **27**: 892-900.

[32] Stephens PW. Phenomenological model of anisotropic peak broadening in powder diffraction. *J Appl Cryst* 1999, **32**: 281-289.